

Electronic Supporting Information

**Synergistic Engineering of Micron-sized Porous Silicon Anodes via Ge
Doping and Liquid Metal Alloy Modification for High-energy-density
Lithium-ion Batteries**

Lin Sun,^{*ab} Lijun Wang,^{ab} Yang Liu,^a Hongyu Wang,^a and Zhong Jin^{*b}

^a *School of Chemistry and Chemical Engineering, Yancheng Institute of Technology, Yancheng, 224051, China.*

^b *State Key Laboratory of Coordination Chemistry, MOE Key Laboratory of Mesoscopic Chemistry, MOE Key Laboratory of High Performance Polymer Materials and Technology, MOE Engineering Research Center of Photoresist Materials, Jiangsu Key Laboratory of Advanced Organic Materials, Tianchang New Materials and Energy Technology Research Center, Institute of Green Chemistry and Engineering, School of Chemistry and Chemical Engineering, Nanjing University, Nanjing, Jiangsu 210023, P. R. China.*

***Electronic Supplementary Information contains Experimental Section, Figures S1-S17
and Table S1.***

1. Experimental Section

1.1 Synthesis of Ge doped pSi (pSi/Ge)

First, 5 g of silicon-aluminum alloy powder ($\text{Al}_{60}\text{Si}_{40}$, Changsha Tianjiu Metal Materials Co., Ltd.) was added into a beaker, which containing 300 mL of 3 M hydrochloric acid (HCl) solution and stirred for 18 hours to completely remove the Al. After the etching reaction was completed, the residual product was centrifuged and washed with deionized water and absolute ethanol several times until the pH of the supernatant above 6.5. The formed powder was vacuum dried at 60 °C overnight to obtain the pSi sample. Afterward, the pSi sample and metal germanium (Ge) powder (Aladdin, 200 mesh, 99.999% purity) were mixed in a planetary ball mill in an atomic ratio of 9:1 for ball milling. Each grinding working time was 100 minutes, and the rest interval was 10 minutes. After working for 10 cycles in this way to obtain the Ge-doped pSi sample (pSi/Ge).

1.2 Synthesis of liquid metal modified pSiGe (pSi/Ge@LM)

First, a metallic gallium-indium-tin alloy was prepared. 0.685 g of Gallium (Ga, 99.99%, Maklin, China), 0.215 g of Indium (In, 99.99%, 200 mesh, Maklin, China), and 0.1 g of Tin (Sn, 99.99%, 200 mesh, Maklin, China) were taken according to the mass ratio of Ga, In, and Sn of 68.5%:21.5%:10%. They were mixed and heated for 1 hour at 85 °C through a water bath to form gallium-indium-tin alloy droplets. Then, 0.5 g of LM was added to 100 ml of isopropanol (99.5%, Xiya, China) under water bath ultrasound and dispersed for 30 minutes. During this period, the ultrasonic temperature was controlled close to 0 °C. After ultrasonic treatment, 0.5 g of pSi/Ge powder was added to the isopropanol solution containing LM and continuous ultrasonic dispersion was carried out for 1 hour. After that, the further continuous stirring was done overnight at 80 °C, the solvent isopropanol was evaporated to dryness, and the pSi/Ge@LM sample was obtained.

1.3 Electrode fabrication

Classical slurry coating and vacuum drying were used to make electrode plates. The active material, Ketjen black (KB) and sodium carboxymethyl cellulose (CMC) were mixed with water in a mass ratio of 7:2:1 to form a slurry with suitable viscosity. A film applicator was used to evenly coat the slurry on a copper foil, and then it was vacuum dried overnight at 80 °C. After drying was completed, a mold was used to evenly cut the copper foil coated with slurry into discs with a diameter of 14 mm. The mass load on each disc was about 1.8 mg cm⁻².

1.4 Materials Characterization

The morphology and microstructure of the obtained products were analyzed using a scanning electron microscope (Field emission SEM, Nova NanoSEM 450) and a transmission electron microscope (TEM, JEM-2100F, Japan). At the same time, an EDS spectrometer (X-MaxN 80TIE250, Oxford Company) was used to record the EDS spectrum of the sample. The XRD pattern was recorded on an X-ray diffractometer (Pan Guang, Cu K α radiation). A 633 nm laser installed on a Raman spectrometer (HORIBA Scientific LabRAM HR Evolution) was used to collect Raman spectra. X-ray photoelectron spectroscopy (XPS) spectra were performed on an Escalab250Xi spectrometer (Thermo Fisher). Thermogravimetric analysis (TGA) was performed at a heating rate of 10 °C per minute in an air atmosphere. Nitrogen adsorption-desorption measurements were performed at 77 K using a Micromeritics ASAP 2020 instrument. Before measurement, all products were degassed under vacuum at 130 °C for 10 hours. The specific surface area was calculated using the Brunauer-Emmett-Teller (BET) method.

1.5 Half-cell assembly and testing

The assembly of the half-cell was carried out in a glove box filled with high-purity argon gas (which needed to meet a water and oxygen content of less than 0.1 ppm). The cutting disc was used as the working electrode and pure lithium foil was used as the counter electrode. The separator used was a porous polypropylene membrane (Celgard 2400), and the electrolyte was composed of LiPF₆ (1 M) dissolved in ethylene carbonate (EC) and diethyl carbonate (DEC) in a volume ratio of 1:1, and vinylene carbonate (VC, 2 wt %) was used as an additive. A battery test system (Neware, Shenzhen, China) was used to evaluate the battery performance in a constant current mode within the specified voltage range (0.01-2.0 V). The specific capacity of the battery was determined according to the content of pure silicon. Electrochemical impedance spectroscopy (EIS) was performed on a CHI660E electrochemical workstation in the range of 0.01 Hz to 100 kHz. Galvanostatic intermittent titration technique (GITT) measurements were also performed using a Neware battery device from 0.01 to 2.0 V. Unless otherwise stated, all electrochemical tests were performed at room temperature.

In addition, in order to improve the ICE of the prepared material electrode, pre-lithiation treatment was carried out. This was achieved by bringing the electrode coated with active material into full contact with lithium foil in the presence of electrolyte for 25 minutes.

1.6 Full cell assembly and testing

A simulated CR2025 button cell was used for full-cell testing, with a commercial NCM811 cathode and pre-lithiated pSi/Ge@LM, and the N/P ratio was maintained at about 1.1. The NCM811 electrode was fabricated by mixing commercial NCM811 material Super P and PVDF binder in a mass ratio of 8:1:1. The assembled full cell was tested

by constant current charging/discharging in the voltage range of 3.0 to 4.3 V, and the specific capacity was calculated according to the weight of the cathode.

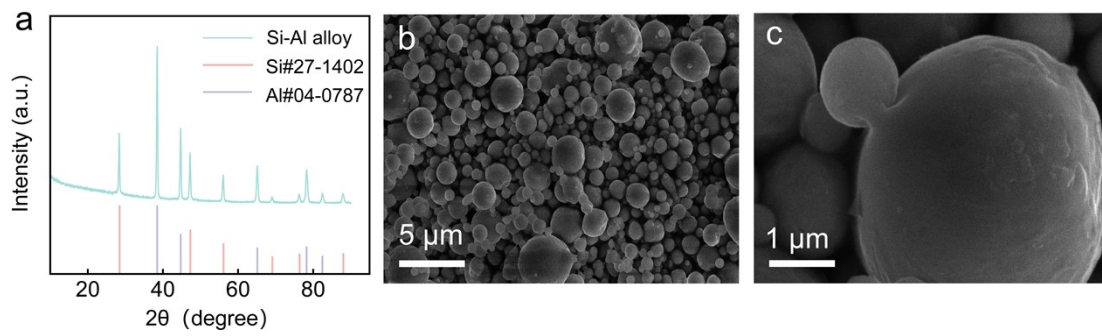


Figure S1. (a) The XRD pattern of $\text{Al}_{60}\text{Si}_{40}$ alloys; (b) and (c) SEM images of $\text{Al}_{60}\text{Si}_{40}$ alloys under different magnifications.

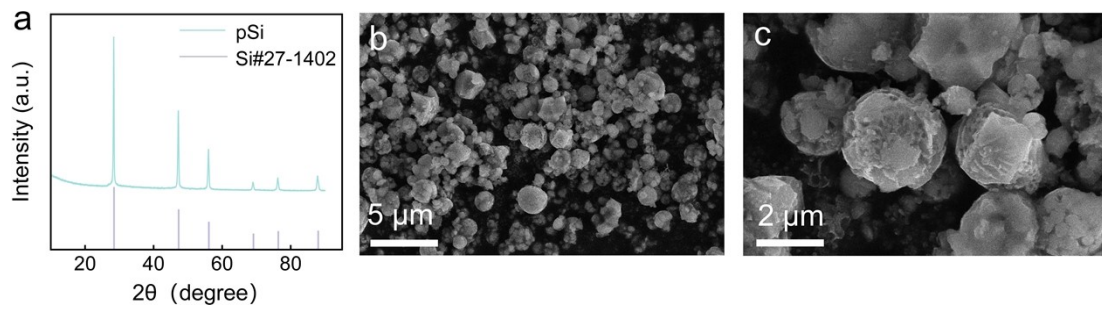


Figure S2. (a) The XRD pattern of pSi; (b) and (c) SEM images of pSi under different magnifications.

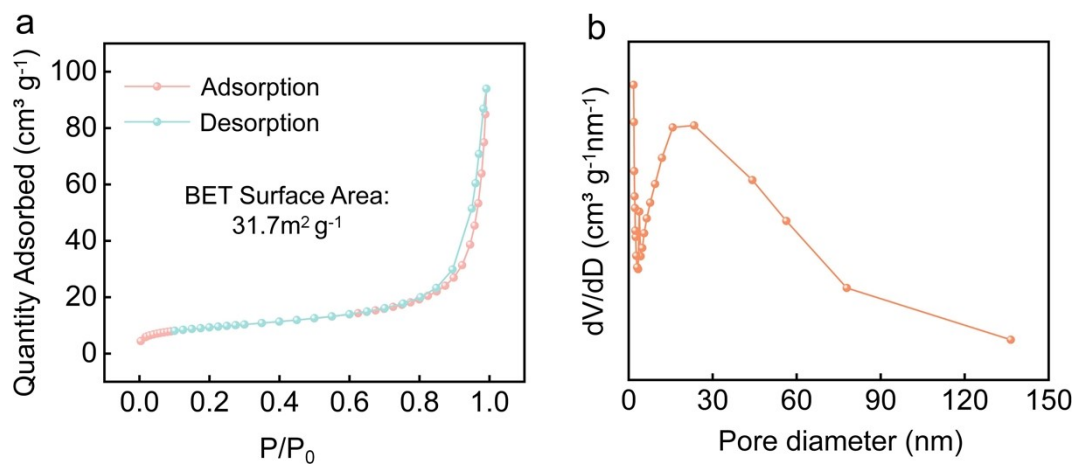


Figure S3. (a) Nitrogen isothermal adsorption-desorption curves of pSi and (b) the pore size distribution curve of pSi.

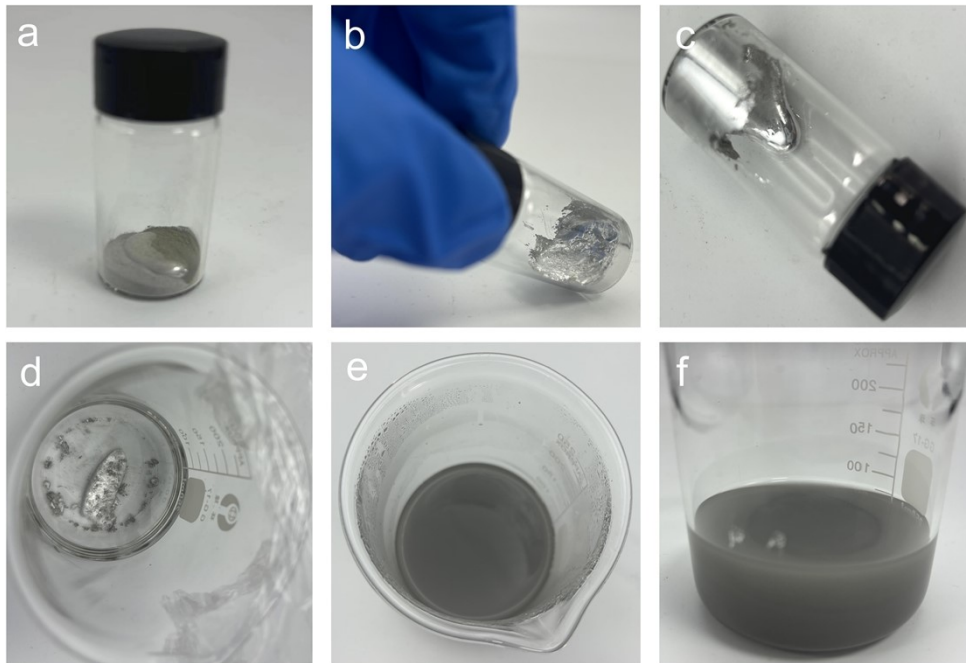


Figure S4. Digital photographs of the GaInSn liquid metal (LM) and its dispersion in isopropanol.

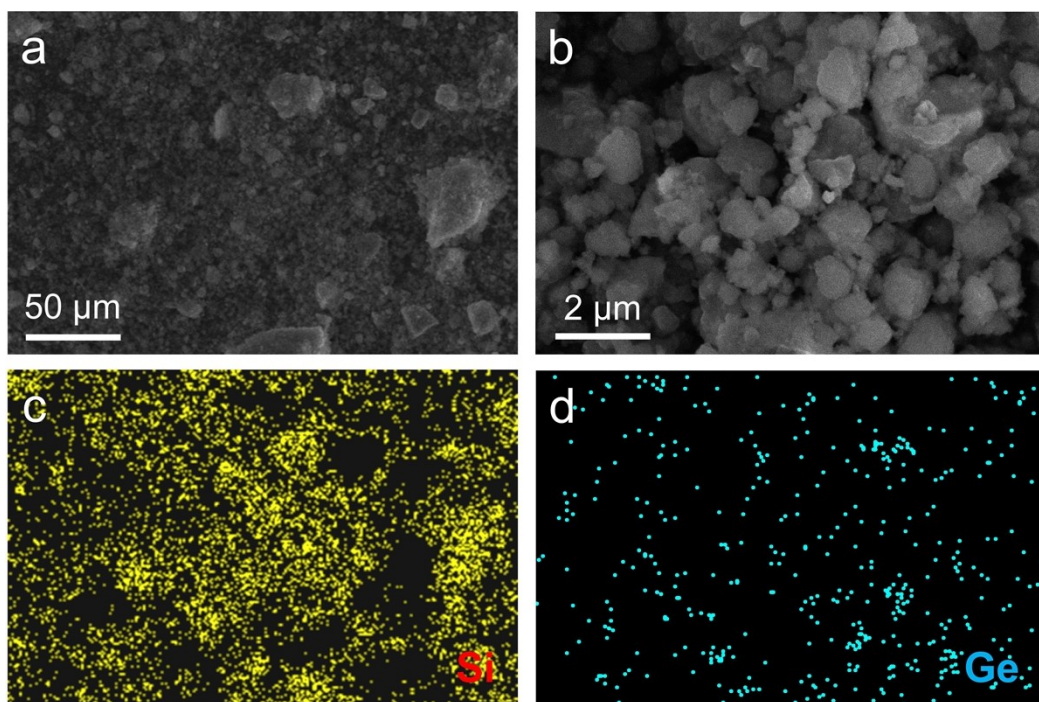


Figure S5. SEM images and element distributions of the pSi/Ge sample.

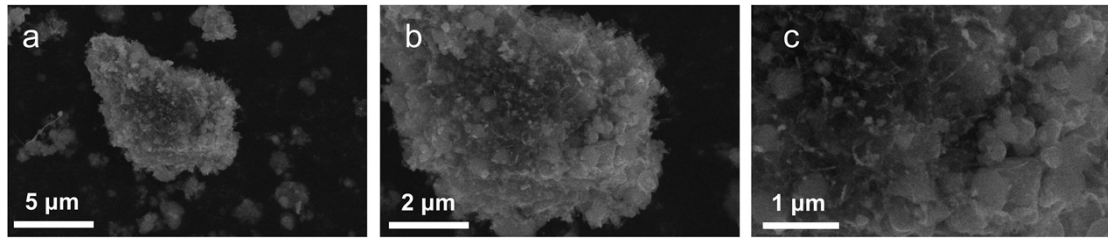


Figure S6. SEM images of the pSi/Ge@LM.

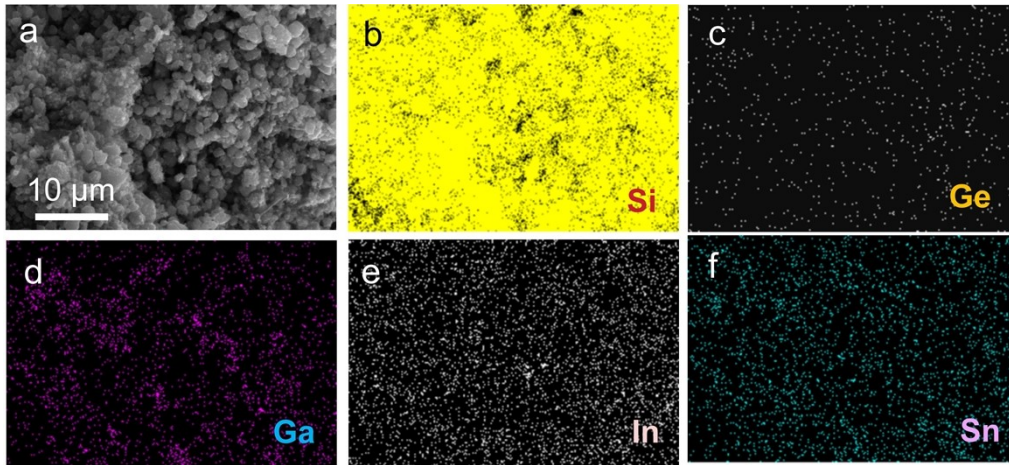


Figure S7. The SEM image and the corresponding elemental mapping of the pSi/Ge@LM.

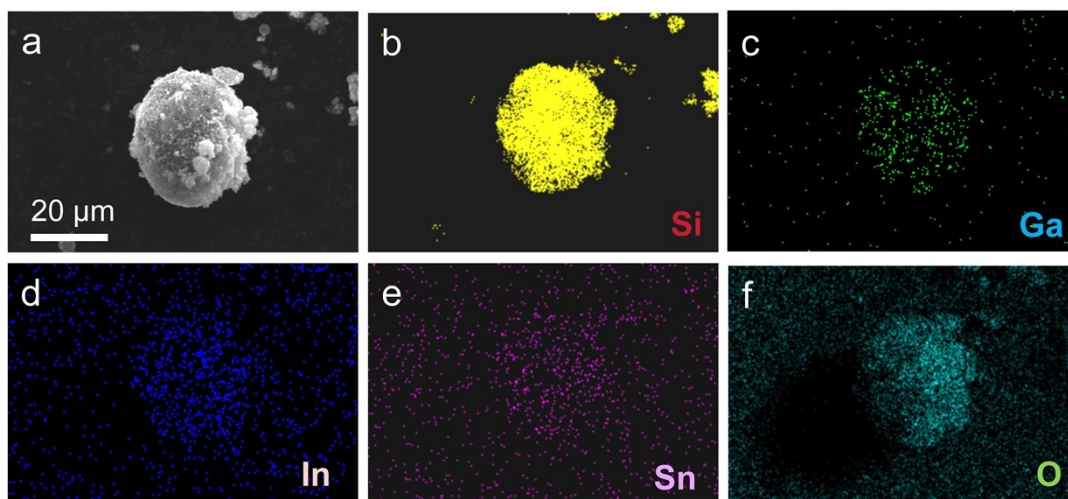


Figure S8. The SEM image and the corresponding elemental mapping of the pSi@LM.

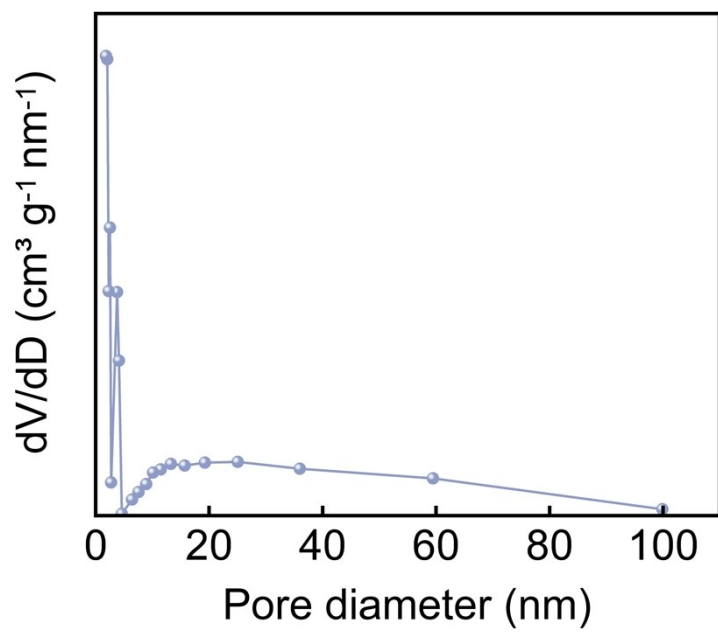


Figure S9. The pore size distribution of the pSi/Ge@LM.

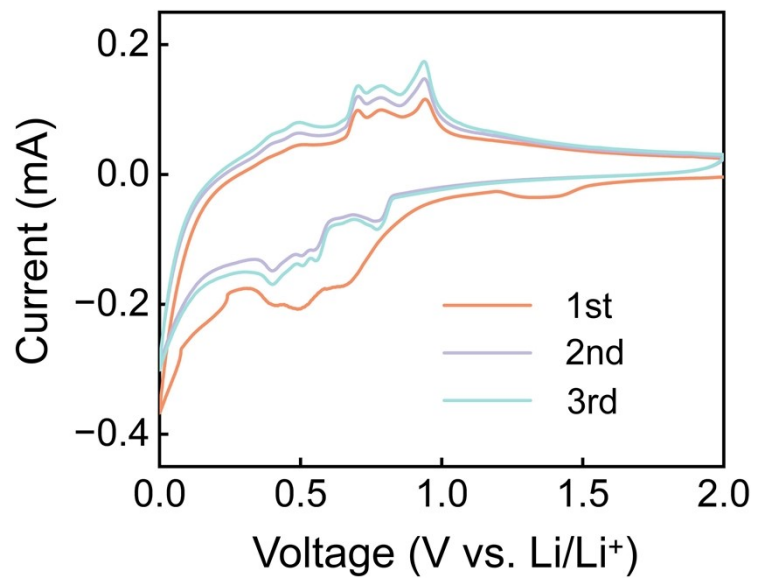


Figure S10. CV curves of the pSi@LM electrode in the first three cycles.

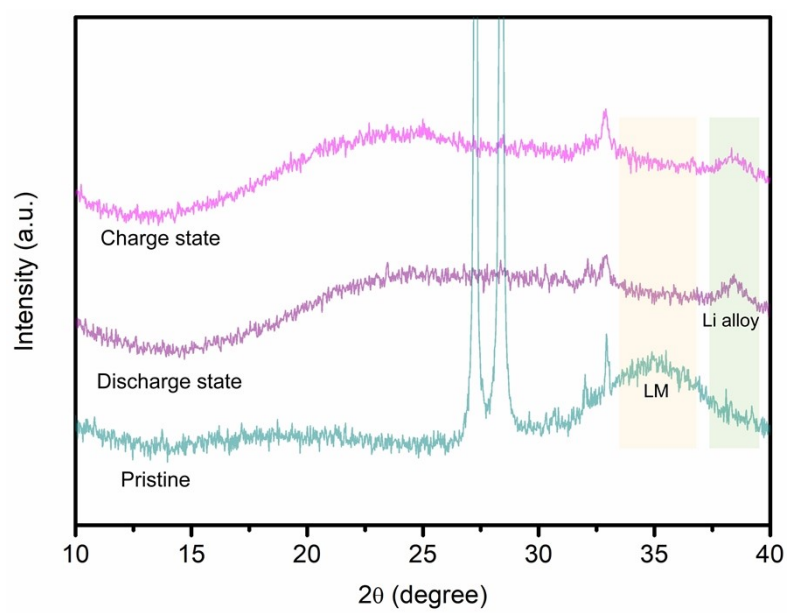


Figure S11. XRD plots of the pSi/Ge@LM electrode in the initial state, discharged state and charged state.

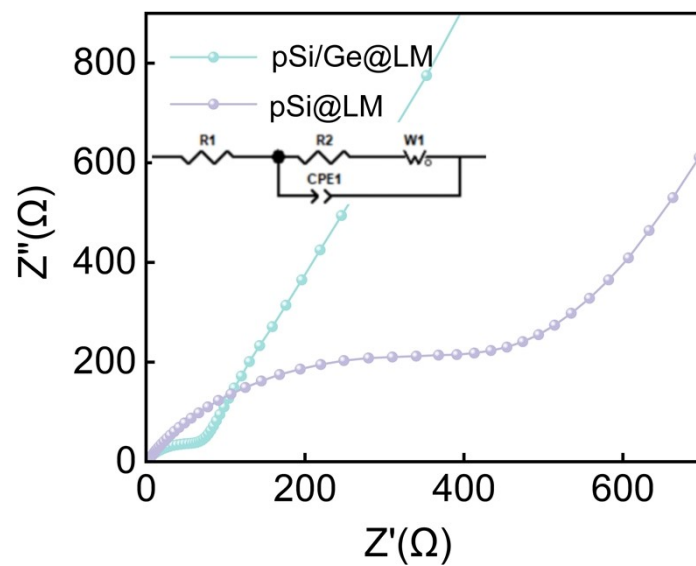


Figure S12. The EIS spectra of the pSi/Ge@LM and pSi@LM electrodes before cycling.

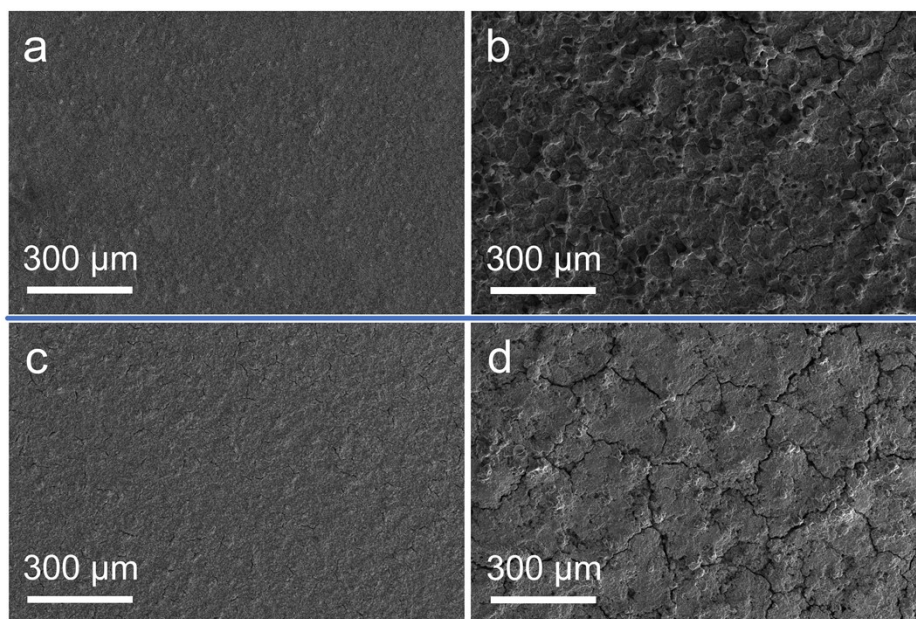


Figure S13. The surface morphologies of the pristine electrodes as well as the pSi/Ge@LM and pSi@LM electrodes after 30 cycles. (a) The pristine pSi/Ge@LM electrode; (b) The pSi/Ge@LM electrode after cycling; (c) The pristine pSi@LM electrode; (d) The pSi@LM electrode after cycling.

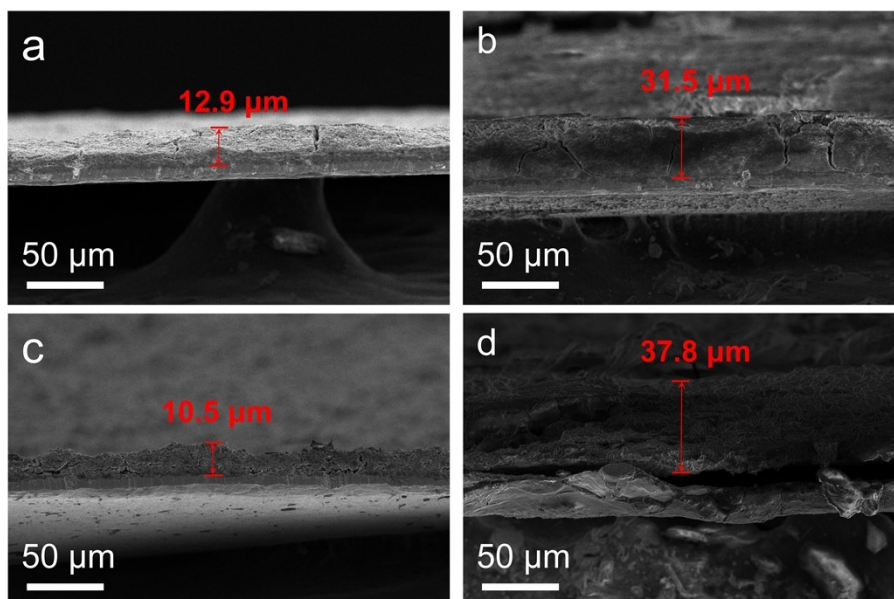


Figure S14. The cross-sectional SEM images of the pristine electrodes as well as the pSi/Ge@LM and pSi@LM electrodes after 30 cycles. (a) The pristine pSi/Ge@LM electrode; (b) The pSi/Ge@LM electrode after cycling; (c) The pristine pSi@LM electrode; (d) The pSi@LM electrode after cycling.

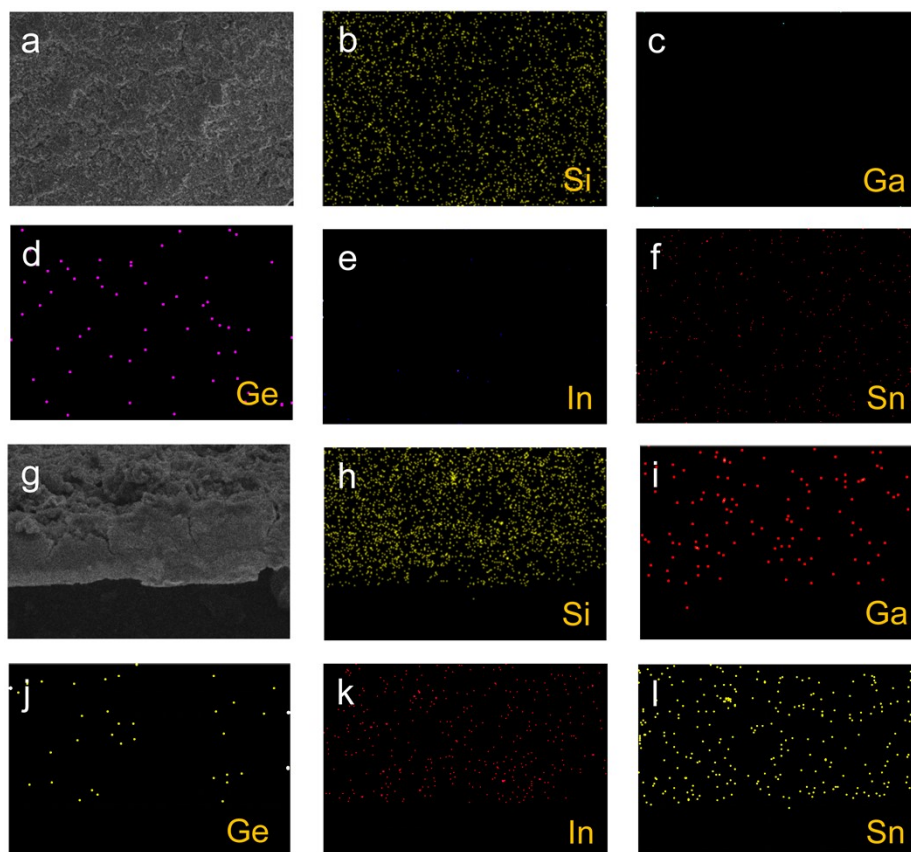


Figure S15. The (a-f) surface morphology and elemental distribution as well as the (g-l) cross-sectional morphology and elemental distribution of the pSi/Ge@LM electrode after cycling.

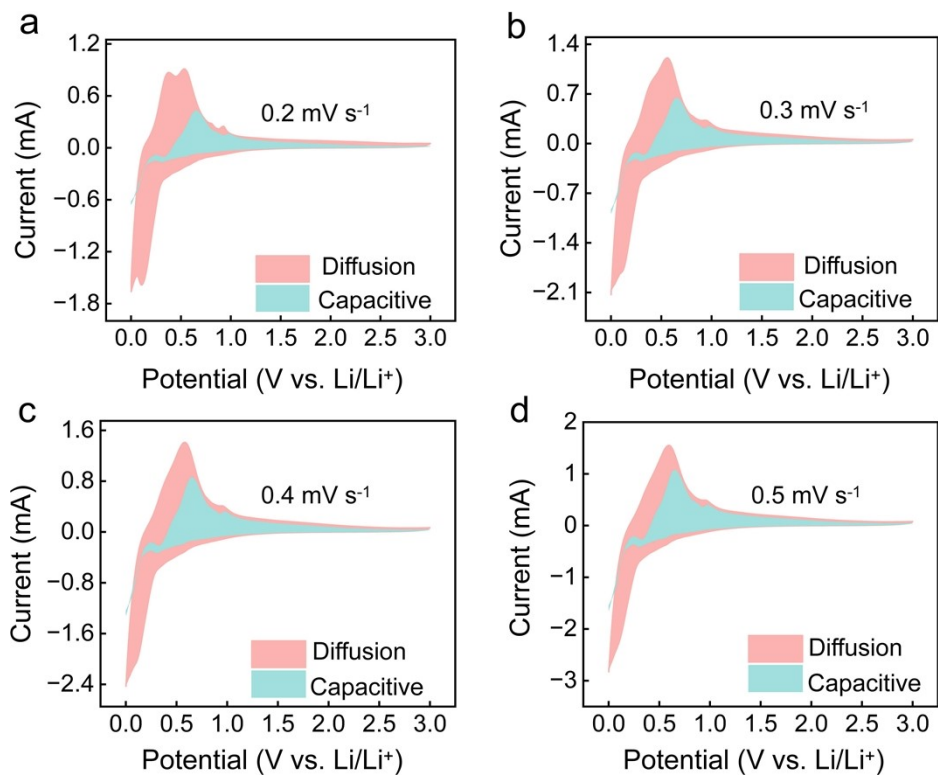


Figure S16. CV curves of the pSi/Ge@LM electrode at different sweep rates.

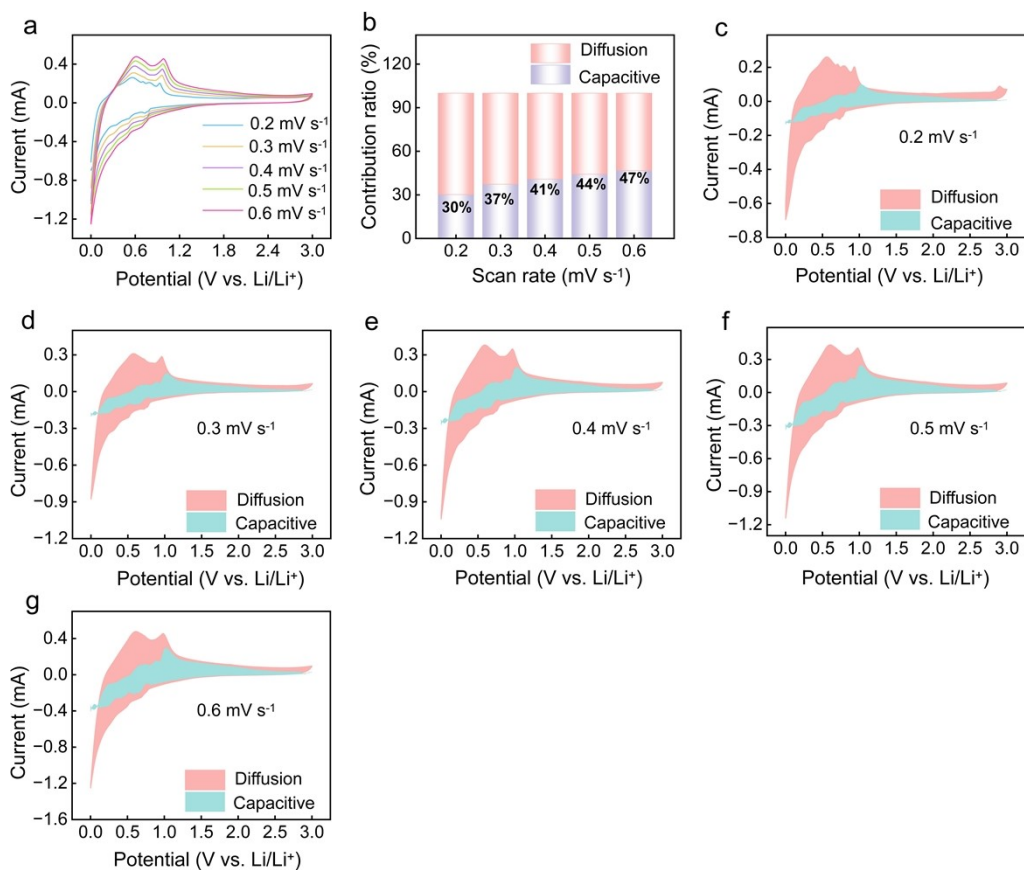


Figure S17. CV tests of the pSi@LM electrode. (a) CV curves at different sweep rates; (b) Contribution ratios of capacitance to charge storage at different sweep rates; (c-g) Proportional areas of the pseudocapacitance and diffusion-controlled charge storage processes in the CV diagrams at different sweep rates.

Table S1. Electrochemical performance comparison of Si-based anodes.

Anodes	Tap density(g cm ⁻³)	Current density	Capacity (mAh g ⁻¹)/cycles	Rate (mAh g ⁻¹ /C or A g ⁻¹)	Ref.
PSi@PA-C	-	0.1 A g ⁻¹	510/100	-	[S1]
Si/Ag@HC	-	0.5 C	997.05/200	Over 600/2 C	[S2]
SiSMPs@TA-2-PAA	-	0.6 A g ⁻¹	2002/100	2303/2 A g ⁻¹	[S3]
STN421	-	0.105 A g ⁻¹	565/120	1100/1.05 A g ⁻¹	[S4]
Si@C/CeO ₂	-	0.1 A g ⁻¹	502.5/180	997.1/1 A g ⁻¹	[S5]
W-Si/NC/Co /CN Ts-2-700	-	0.2 A g ⁻¹	1039/100	485/1 A g ⁻¹	[S6]
DSM-Si	1.001	0.1 A g ⁻¹	957/400	-	[S7]
Fe-Si@MLC-2	-	0.5 A g ⁻¹	805.9/200	455.6/10 A g ⁻¹	[S8]
Vg-PMSi@Ag	-	2 A g ⁻¹	1403.9/100	943.8/6 A g ⁻¹	[S9]
PSi1@SiO ₂ @C	-	0.1 A g ⁻¹	933.3/100	381.9/3 A g ⁻¹	[S10]
FeCuSi	0.8	0.5 C	1287/50	-	[S11]
Si@Void@C Cluster	0.91	1 C	1250/1400	880/4 C	[S12]
Si@TiO ₂ Cluster	1.4	0.5C	990/1500	-	[S13]
nano-/micro Si/C composite	0.84	0.42 A g ⁻¹	872/300	510/13 A g ⁻¹	[S14]
Si/Ge@LM	1.67	0.2 A g ⁻¹	1908/100	985/3 A g ⁻¹	This work

References

- S1. K. Wang, B. Xue, Y. Tan, J. Sun, Q. Li, S. Shi and P. Li, *Journal of Cleaner Production*, 2019, **239**, 117997.
- S2. F. Chen, J. Chen, G. Xu, C. Jin, H. Ma, L. Wen, C. Tu, F. Sun, Y. Li, H. Li, L. Zhou and Z. Yue, *Ionics*, 2024, **30**, 7861-7868.
- S3. M. Tian and P. Wu, *ACS Applied Energy Materials*, 2019, **2**, 5066-5073.
- S4. Y. Ma, H. Li, Q. Li, J. Zhou, Z. Cai, S. Wang, M. Yu, C. Liu, G. Song and C. Wen, *Journal of the American Ceramic Society*, 2024, **107**, 276-284.
- S5. J. Wang, Y. Mai, P. Yang, D. Guo, R. Sun, F. Wu, X. Dai, Y. Gu, H. Chen and Y. Cheng, *Applied Surface Science*, 2023, **613**, 156044.
- S6. Z. Hu, T. Jiang and Y. Zhou, *Materials Today Communications*, 2024, **40**, 110019.

-
- S7. Y. Yang, C. Ni, M. Gao, J. Wang, Y. Liu and H. Pan, *Energy Storage Materials*, 2018, **14**, 279-288.
- S8. M. Li, J. Qiu, S. Zhang, P. Zhao, Z. Jin, A. Wang, Y. Wang, Y. Yang and H. Ming, *Journal of Energy Chemistry*, 2020, **50**, 286-295.
- S9. Y. Mo, S. Li and J. Yu, *ACS Applied Nano Materials*, 2022, **5**, 8205-8213.
- S10. K. Wang, Y. Tan, P. Li, B. Xue and J. Sun, *ACS Applied Materials & Interfaces*, 2019, **11**, 37732-37740.
- S11. S. Chae, M. Ko, S. Park, N. Kim, J. Ma and J. Cho, *Energy & Environmental Science*, 2016, **9**, 1251-1257.
- S12. D. Lin, Z. Lu, P.-C. Hsu, H. R. Lee, N. Liu, J. Zhao, H. Wang, C. Liu and Y. Cui, *Energy & Environmental Science*, 2015, **8**, 2371-2376.
- S13. Y. Jin, S. Li, A. Kushima, X. Zheng, Y. Sun, J. Xie, J. Sun, W. Xue, G. Zhou, J. Wu, F. Shi, R. Zhang, Z. Zhu, K. So, Y. Cui and J. Li, *Energy & Environmental Science*, 2017, **10**, 580-592.
- S14. J. Liu, Q. Zhang, Z.-Y. Wu, J. T. Li, L. Huang and S. G. Sun, *ChemElectroChem*, 2015, **2**.